HEFAT2007
5th International Conference on Heat Transfer, Fluid Mechanics and Thermodynamics
Sun City, South Africa
Paper number: LL1

VORTICITY ESTIMATION UTILIZING THE ROTATION OF FINITE LINE SEGMENTS

Langston, L. S.*
University of Connecticut
Mechanical Engineering Department
Storrs, CT 06269 USA
langston@engr.uconn.edu
* Author for correspondence

Abraham, B. M.
Applied Physical Sciences Corp.
Groton, CT 06340 USA
babraham@aphysci.com

ABSTRACT

In a fluid flow field where velocities are measured or numerically calculated, the vorticity value at a point in the field is usually estimated by approximating partial derivatives of velocity with ratios of velocity differences and spatial differences. Based on the fundamental definition of rotation, this paper presents an alternate approach to estimate vorticity, by using the instantaneous relative angular velocity of finite line segments radiating from the point to adjacent points in the fluid.

The number, length and placement of line segments are varied to find their effects on predicted vorticity values in four laminar flow fields with known vorticity. Equations are also derived for a configuration consisting of four independent finite line segments which has application to a square numerical velocity mesh and to instrumentation such as hot wire vorticity probes and vane vorticity meters. The results presented are relevant to both experimental and computational fluid mechanics.

NOMENCLATURE

Latin

- a - constant for stagnation flow (Equation (8))
- f - Blasius function, $f = f(\eta)$
- i - point i (Figure 3)
- k - free vortex strength
- ℓ - ideal vorticity meter vane width (Figure 4)
- n - number of line segments, vanes
- n' - number of line segments (unequal length)
- 0 - point 0 (Figs. 1-4)
- r_0 - radius of point 0 in xyz coordinates (Figure 3)
- R_x - Reynolds number based on $u_\infty x/\nu$
- s - length of line segment (Figs. 1-4)
- s' - s/ r_0
- s^* - s/δ
- t - time or instant, t
- u - velocity in the x- direction
- v - velocity in the y- direction
- w - velocity in the z- direction
- W - solid body rotation constant
- x,y,z - fixed Cartesian coordinate system (Figs. 1,3,8)
- x',y',z' - Cartesian coordinate system, fixed at point 0 (Figures 1, 3, 4)
- y^* - y/δ

Greek

- δ - boundary layer thickness
- ζ_0 - vorticity component in the z-direction at point 0
- ζ_0^* - $\zeta_0\delta/ u_\infty$
- Z_0^* - estimated vorticity component in the Z-direction $(2\Omega_0\delta/ u_\infty)$
- η - Blasius similarity variable, $y\sqrt{u_\infty / 2\nu x}$
- η_0 - vorticity component in the y-direction at point 0
- θ - angle between x-axis and line segment (Figs. 2-4)
- ν - kinematic viscosity
- ξ_0 - vorticity component in the z-direction at point 0
- ϕ_0 - angle between r_0 and x-axis (Figure 3)
- ω_0 - rotation at point 0
- ω_{0i} - angular velocity of line segment 0i about point 0
- Ω_0 - estimated rotation at point 0
- Ω_0^* - $\Omega_0 r_0^2 /k$
- ∞ - infinity

Subscripts

- i - point i
- n - normal
- 0 - point 0
- 0i - line segment 0i
- x - x-direction
- 1,2,3,4 - points
- 01,02,..0i - line segments
- ∞ - free stream condition

INTRODUCTION

The Cauchy-Stokes Decomposition Theorem postulates that the kinematics of a fluid particle can be broken down into four component motions: Translation, dilation, angular deformation and rotation. The first three are used directly in the derivation of the Navier-Stokes equations, while the consequences of rotation, or vorticity, are neglected.

However, vorticity has been called the key to fluid mechanics by Shercliff (1977) and others. Endeavors to measure, calculate and predict vorticity are and have been a focus for many fluid mechanics researchers. Monographs devoted to the subject of vorticity range from that of Truesdell (1954) to Saffman (1992). Vorticity determination has been greatly facilitated in recent years by the development of powerful computer and numerical methods, and by the introduction of new experimental instruments and techniques. In the very active area of turbulence research, recent work on coherent or organized structures has fostered vorticity measurement and calculation. Wallace and Foss (1995) have called vorticity a defining property of turbulence.

Originally defined by Lamb (1932), vorticity is twice the instantaneous rotation at a point in a moving fluid. The definition of fluid rotation on which this paper is based is Cauchy's First Interpretation of Rotation as given by Truesdell (1954). Consider a point 0 in a moving fluid. At the instant t, it is located at (x_0, y_0, z_0) of the fixed Cartesian coordinate system in Figure 1, and all fluid points on the surface of a sphere of radius s centered at 0 (the red sphere in Figure 1) are imagined to be connected to 0 by line segments. (Such a contrivance might look like a "Koosh" ball, the popular toy ball constructed of several thousand rubber filaments radiating from a center (point 0)). The average of the angular velocities of all of the imaginary line segments of length s relative to point 0 at the instant t, is defined as the rotation at 0. Rotation then, is in no way, simple solid body rotation of fluid points about point 0.

The envelopes of the projection of the radial line segments onto each of the three coordinate planes (x=0, y=0 and z=0) are the cylinders shown in Figure 1. The average angular velocity of the projected line segments in each coordinate plane gives a component of rotation. Multiplication of each by the Lamb factor of two yields the vorticity components at 0, given by the arrows in Figure 1 as ζ_0, η_0, ξ_0.

If s is taken to be the infinitesimal ds, the velocity field around 0 can be expressed as a Taylor series, with higher order terms neglected. Incorporation of the infinitesmality of the line segment s and the abbreviated Taylor series into Cauchy's original definition of rotation (e.g. see Shercliff (1977)) results in the familiar expressions for the components of vorticity,

$$\zeta_0 = \frac{\partial v_0}{\partial x} - \frac{\partial u_0}{\partial y} \qquad (1)$$

$$\eta_0 = \frac{\partial u_0}{\partial z} - \frac{\partial w_0}{\partial x} \quad , \qquad (2)$$

and

$$\xi_0 = \frac{\partial w_0}{\partial y} - \frac{\partial v_0}{\partial z} \quad , \qquad (3)$$

where u_0, v_0, w_0 are the velocities at point 0 in the x, y and z directions. If an analytical expression accurately describes a velocity field of interest, the vorticity can easily be calculated by carrying out the differentiation in Equations (1) - (3). This is usually not the case (e.g. most flows are geometrically complex and/or turbulent) and, short of solving the Navier Stokes equations rewritten as the vorticity transport equations, a physical or computational velocity grid or mesh is typically constructed. Figure 2 shows a two-dimension velocity mesh in the z=0 plane with sxs square openings and mesh point 0 surrounded by mesh points 1 – 4 and 1′ – 4′. Velocities (u and v in the Figure 2 mesh) at each mesh points can be obtained by either:

1) Solution of the governing equations by finite difference methods (or by some other numerical method).
2) Experimental measurement. For example velocities at mesh points can be measured by using pressure probes, laser-doppler anemometry, or hot wire anemometry. A Kovaszny - type four-sensor hot wire probe is an example of the latter. It is used to measure velocity differences to estimate vorticity. The outline of an upstream view of the four hot wires (each inclined at a 45° angle to the probe axis) is sketched in Figure 2. More details of this vorticity probe are given by Wallace and Foss (1995).

Once the velocity mesh is synthesized the vorticity values at mesh points can be estimated by using appropriate velocity differences and mesh point distances to approximate the derivatives in Equations (1) - (3). However this usual approach to determine vorticity is based on the use of finite distances and finite velocities to approximate partial derivatives which arose from a vorticity derivation based on infinitesimal differences (Shercliff (1977)).

For example, using finite differencing to represent ζ_o in Equation (1) for point 0 in Figure 2 (for θ_1=0) results in,

$$\zeta_o = \frac{(v_1 - v_o) - (u_2 - u_o)}{s} \qquad (1'a)$$

for forward differencing,

$$\zeta_o = \frac{(v_o - v_3) - (u_o - u_4)}{s}. \qquad (1'b)$$

for backward differencing, and

$$\zeta_o = \frac{(v_1 - v_3) - (u_2 - u_4)}{2\,s}. \qquad (1'c)$$

for central differencing. Equations (1'a), (1'b) and (1'c) are each numerical representations of the partial differential equation (1), but which one is the closest representation of the actual Cauchy definition of fluid rotation?

A more straightforward approach to the estimation of vorticity is to go back to the fundamental kinematics definition of rotation, based on the rotation of finite line segments. In this paper, such a finite line segment analysis is presented for the estimation of vorticity. What result are quantitative criteria on how large a vorticity measurement device can be or how large a measurement or calculation mesh can be selected to yield accurate vorticity values. This finite line segment approach also yields insights into the number and location of sensors and mesh points needed to get an accurate representation of vorticity at a point in a given flow field. Lastly, the finite line analysis answers the question of which finite difference method, (1'a), (1'b) or (1'c) is the most accurate.

FINITE LINE SEGMENT ROTATION ANALYSIS

Cauchy's First Interpretation of Rotation given by Truesdell (1950) and discussed in the Introduction will be used to calculate the rotation at point 0 of a two-dimensional flow field at an instant t, shown in Figure 3. (Other components of rotation and vorticity, (as shown in Figure 1) can be calculated in a similar fashion for a full three-dimensional flow.) At t, i is a neighboring point of 0 in the fluid , defining the instantaneous finite line segment 0i. The rotation of the fluid surrounding point 0 is defined as the average rate of right-handed rotation (+θ as shown in the figure) of all line segments 0i of length s in the xy plane about 0, expressed as,

$$\omega_0 = \frac{1}{2\pi}\int_0^{2\pi} \omega_{0i} d\theta = \frac{1}{2}\zeta_0 , \qquad (4)$$

where ω_0 is the instantaneous average rotation of fluid about 0 at radius s, ω_{0i} is the instantaneous rate of rotation of finite line segment 0i about point 0, and ζ_0 is the vorticity in the z-direction, shown in Figure 1.

The finite line segment 0i of length s has no interaction with the fluid between points 0 and i. Its rate of rotation ω_{0i} serves to show how fast point i in the fluid rotates with respect to point 0, at instant t. Thus ω_{0i} is given by the difference in the velocities normal to the line segment, v_{ni} - v_{no} divided by length s. Putting this in terms of the Cartesian xy velocity components shown in Figure 3 results in,

$$\omega_{0i} = \frac{v_{ni} - v_{n0}}{s} = \frac{1}{s}\left[(v_i - v_0)\cos\theta_i - (u_i - u_0)\sin\theta_i\right] , \qquad (5)$$

where θ_i is the angle at which 0i is inclined to the Cartesian coordinate system x'y' centered at point 0 (+ in a counter clockwise direction) at time t.

If u and v are known analytical functions, Equations (4) and (5) can be combined and integrated to give a value of ω_0 , the rotation of fluid particles at radius s about the point 0 at time t. Note that if this results in an analytic expression for ω_0, the expression will not contain u_o or v_o since these will cancel out in the integration taken over $0 \le \theta \le 2\pi$.

Alternately, an "ideal" rotation or vorticity meter could be constructed to measure ω_0 at point 0, as shown in Figure 4. It consists of a large number (n) of small (massless) radial vanes ($\ell << s$) with vane centers mounted at radius s on thin (dragless) rigid wire struts, each rotating at ω_{0i} (on a frictionless bearing) independently of the others. At any instant t, the estimate of the rotation at 0 would be given by,

$$\Omega_0 = \frac{\sum_{i=1}^{n} \omega_{0i}}{n} . \qquad (6)$$

As $n \to \infty$, Ω_0 given by (6) approaches the value given by (4), $\omega_0 = 1/2\zeta_0$. Mounting this ideal vorticity meter along the x' and y' axes in Figure 1 would yield η_0 and ξ_0, the other two Cartesian components of the vorticity vector at 0, for large n.

Real (non-ideal) vane vorticity meters frequently are used to study rotational flows, such as wing tip vortices and boundary layers. A four-vaned vorticity meter used by McCormick (1968) consists of four radial vanes rigidly mounted 90^o apart on a shaft. A direct comparison of this non-ideal vorticity meter with the ideal vorticity meter of Figure 4, raises questions about how closely the rotation of four fixed, interdependent vanes approximates a true measure of ω_0. The McCormick device is a turbine, rotated by lift forces. More recently Willey (1985) tested a four element vorticity meter that rotated by drag forces. Consideration of Figure 4 shows that neither of these devices closely approximates the combined motion of four independent, massless and dragless vanes of an ideal meter.

Thus Equation (6), which approximates Equation (4) by averaging instantaneous rotation rates of n finite line segments at point 0, can be evaluated from an experiment (e.g. by use of a n-vaned vorticity meter shown in Figure 4) or from a velocity field (e.g. by mesh point velocities obtained from a numerical solution or by measurements.) Three questions arise:

1) How many line segments (n) are needed to get an accurate instantaneous value of Ω_0 (i.e. $\Omega_0 \approx \omega_0$)?
2) How long should the line segments, s, be relative to the flow field?
3) At what angles (θ_i) should the n line segments be placed?

The answers to these three questions will of course depend on the flow field itself. Given velocities u and v, the variables n, s and θ_i can be varied over ranges, using Equations (5) and (6). Since the most common applications involve n=4 (e.g., the four sensor hot wire probe, the McCormick and Willey meters and a square finite difference mesh) it is convenient to derive an expression for Ω_0 in (6) for this common case.

The angular velocities of the four independent finite line segments in Figure 2 are $\omega_{01}(\theta_1)$, $\omega_{02}(\theta_1+\pi/2)$, $\omega_{03}(\theta_1+\pi)$, and $\omega_{04}(\theta_1+3\pi/2)$. Substitution of these into Equation (5) and combining them into Equation (6) for n=4, yields (using suitable trigonometric identities),

$$\Omega_0 = \frac{1}{4s}\{[(v_1 - v_3) + (u_4 - u_2)] \cos\theta_1 + [(v_4 - v_2) + (u_3 - u_1)]\sin\theta_1\}. \quad (7)$$

The rotation at point 0, $\omega_0 = 1/2\zeta_0$, is now approximated in (7) by the average instantaneous angular velocity, Ω_0, of the four finite (length s) line segments, written in terms of their Cartesian tip velocities referenced to the fixed xy coordinate system. Because of the finite line segments, Ω_0 is also a function of θ_1, which characterizes the instantaneous angular position of the four line segment array at 0 in Figure 2.

The accuracy of the finite difference vorticity equations (1'a), (1'b) and (1'c) can now be evaluated using fig. 2 and Equation 7. Setting $\theta_1=0$ and using $\zeta_o=2\Omega_o$, Equation 7 becomes,

$$\zeta_o = \frac{(v_1 - v_3) - (u_2 - u_4)}{2s}, \quad (7')$$

which is identical to Equation (1'c). Thus, central differencing most accurately represents fluid rotation, while forward and backward differencing differ from (7') by a factor of two, and involved different velocity components.

ROTATION TEST CASE RESULTS

The accuracy of vorticity determination at a point in a moving fluid by the use of a four-vaned vorticity meter, a four-element hot wire vorticity probe or a square velocity grid can be evaluated by using Equation (7'). Using laminar two-dimensional flows for which closed-form solutions exist, Ω_0 from (7) can be evaluated at points in the flow field and compared to ω_0, where ω_0 can be calculated from Equation (1) or (4), or both. In this way the effects of limiting the number of finite line segments to n=4, and the effect of sensor or mesh size (s) and placement can be evaluated.

Four laminar two dimensional flows will be used:

1) Potential stagnation flow ($\zeta_0 = 0$)
2) Solid body rotation flow (ζ_0 is constant).
3) Free vortex flow ($\zeta_0 = 0$ except at the origin).
4) Blasius boundary layer flow (ζ_0 varies).

In addition, one turbulent, two-dimensional flow will be considered:

5) Direct Numerical Simulation (DNS) of flow over a thin, flexible plate or "flag".

These simple two-dimensional test case flows (#1 – 4) can also be looked upon as the x-y components of a three-dimensional flow. The two inviscid flows (case 1) and 3)) can be considered to be superimposed on a uniform flow in the z-direction. Similarly, case 2) , the fully viscous solid body rotation, could be added to a uniform z-direction flow. (Vorticity probes are commonly calibrated by rotating the probe about its axis in a known uniform axial flow.) Case 4 could represent the two-dimensional part of a laminar three-dimensional Loos-Sowerby boundary layer (as discussed by Panton (1984)). The turbulent example will show that the trends observed via the laminar cases also are consistent with the vorticity estimated from a turbulent velocity field.

1) Potential Stagnation Flow

The Cartesian velocity field in plane potential stagnation flow is given by,

$$u = ax,\ v = -ay. \quad (8)$$

where a is constant. This is an inviscid, irrotational flow, and substitution of (8) into Equation (1) will verify that at any point 0 in the flow field, $\omega_0 = 0$. Rewriting (8) in terms of the geometry in Figure 2, the velocities at point 1 for the potential stagnation flow are,

$$u_1 = ax_1 = a(r_0\cos\phi_0 + s\cos\theta_1)$$
$$v_1 = -ay_1 = -a(r_0\sin\phi_0 + s\sin\theta_1). \quad (9)$$

The velocities at points 2, 3 and 4 can be easily found by substituting $(\theta_1+\pi/2)$, $(\theta_1+\pi)$, and $(\theta_1+3\pi/2)$ into (9). Substitution of these velocities into Equation (7) results in $\Omega_0 = 0$ everywhere in the flow field, independent of the line segment length s. Thus, any size four line segment device or mesh would yield a correct vorticity value, ($\Omega_0 = \omega_0 = 0$), of ζ_0, anywhere in this pure potential flow field.

2) Solid Body Rotation

In solid body rotation the entire flow field rotates in the xy plane about the z-axis at constant angular velocity, W. The velocity is tangential to the circular streamlines and proportional to the streamline radius. The cartesian velocities in this rotational viscous flow are,

$$u = -Wr\sin\phi$$
$$v = Wr\cos\phi. \quad (10)$$

where r and ϕ are defined in Figure 2.

Rewriting (10) in terms of the four line segments in Figure 2, the velocities at point 1 for solid body rotation are,

$$u_1 = -W(r_0\sin\phi_0 + s\sin\theta_1)$$
$$v_1 = W(r_0\cos\phi_0 + s\cos\theta_1). \quad (11)$$

The velocities at points 2, 3 and 4 can be found as before, using (11). Substitution into Equation (7) results in $\Omega_0 = W$. This is exactly what Equations (10) and (1) yield, so that for solid body rotation, $\Omega_0 = \omega_0 = W$ and the vorticity is $\zeta_0 = 2W$, which is constant everywhere in the flow field.

Again, any size four-element device or mesh (Figure 2) will yield a correct value of ω_0 in this constant (non-zero) vorticity flow field. Vorticity probes have been calibrated by rotating the probe about its axis facing into a uniform flow (Kovasznay (1954)). The result obtained from Equation (7) would indicate such a procedure is a valid one, and one that would be independent of the probe size (disregarding probe size effects on the flow field itself).

3) *Free Vortex Flow*

Circular streamlines also characterize free vortex flow, but this rotating flow has a tangential velocity that is inversely proportional to streamline radius. The Cartesian velocities in this irrotational (except at the origin) inviscid flow are,

$$u = -\frac{k}{r}\sin\phi \qquad v = \frac{k}{r}\cos\phi \qquad (12)$$

where r and ϕ are defined in Figure 3 and k is the vortex strength (a constant). Substitution of (12) into Equation (1) shows that $\omega_0 = 0$ anywhere in the region r > 0. A singular point exists at r = 0, where the tangential velocity is infinite and the vorticity is nonzero in this inviscid and otherwise irrotational ($\zeta_0 = 0$) flow.

Rewriting (12) in terms of the Figure 3 geometry, the Cartesian velocities for point i are,

$$u_i = \frac{k}{r_0}\left[\frac{\sin\phi_0 + s'\sin\theta_i}{(\cos\phi_0 + s'\cos\theta_i)^2 + (\sin\phi_0 + s'\sin\theta_i)^2}\right]$$

$$v_i = \frac{k}{r_o}\left[\frac{\cos\phi_0 + s'\cos\theta_i}{(\cos\phi_0 + s'\cos\theta_i)^2 + (\sin\phi_0 + s'\sin\theta_i)^2}\right] \qquad (13)$$

where r_0, ϕ_0, and θ_i are shown in Figure 3 and $s' = s/r_0$.

Free vortex flow with its singularity at r = 0 presents a more complex velocity field for a finite size vorticity meter or mesh. This can be seen by combining Equation (13) (and corresponding expressions for u_0 and v_0) with Equation (5) to get an expression for ω_{0i}, the rate of rotation of a single finite line segment 0i , in the free vortex flow field. The result is,

$$\omega_{0i}^* = \frac{\omega_{0i} r_0^2}{k} = \left[\frac{1 - \cos\theta_i (s' + 2\cos\theta_i)}{1 + 2s'\cos\theta_i + (s')^2}\right], \qquad (14)$$

where ω_{0i}^* is ω_{0i} nondimensionalized by k/r_o^2, the rate of rotation of point 0 around the xy origin, and $s' = s/r_0$, as before. Equation (14) has been derived for $\phi_0 = 0$ (see Figure 3) only because ω_{0i}^* has the same behavior at other values of ϕ (at constant r_0) due to the free vortex flow field symmetry.

Equation (14) is plotted in Figure 5 with ω_{0i}^* as a function of θ_i for various values of s'. For s' = 0 (a case of a vanishingly small line segment 0i or a case of $r_0 >> s$), Equation (14) reduces to,

$$\omega_0^*\big|_{s'=0} = 1 - 2\cos^2\theta_i = -\cos 2\theta_i . \qquad (15)$$

The simple cosine function in Equation (15) is plotted in Figure 5 and clearly shows that the areas above and below the ω_{0i}^* axis cancel so that the average value of ω_{0i}^* is zero (i.e. zero vorticity) at r_0, for $s' \rightarrow 0$. The finite line segment approach expounded here allows one to see the actual distribution of neighboring point rotational rates about point 0. The infinitesimal approach, used to derive Equation (1) (Shercliff (1977)), is independent of θ_i, hence does not provide this distribution information.

For values of s'>0, plots of Equation (14) in Figure 5 show some elucidative line segment rotational distributions about point 0 in this free vortex flow. For example, the curve for s' = 0.4 shows that the line segment 0i starts out with a clockwise rotation rate of $\omega_{0i}^* = -0.7$ at $\theta_i = 0$. As θ_i is increased, the rotation rate goes to zero at about 60°, and then becomes counterclockwise between 60° and 160°, reaching a maximum of $\omega_{0i}^* = 1.02$ at about 110°. As line segment 0i swings past $\theta_i = 160°$ it approaches the free vortex singularity at the xy origin, which of course, is a region of steep velocity gradients. This causes ω_{0i}^* to become strongly negative (clockwise rotation) until it reaches $\omega_{0i}^* = -1.7$ at $\theta_i = 180°$ after which it retraces in reverse the 0° to 180° sequence as line segment 0i is rotated full cycle to 360°.

As will be shown later, the average rate of rotation for all s' < 1.0 (the net area under the s'curves) is zero (i.e. zero vorticity). It will also be shown that the four line segment configuration of Figure 2 will not yield zero vorticity, for values of s' large enough to have individual line segment rotation rates significantly effected by the large velocity gradients near the singularity. Some fluid mechanics textbooks use behavior of a pair of crossed lines (same configuration as shown in Figure 2) in a free vortex flow to illustrate irrotational flow. A student may be perplexed by the illustration, because as Figure 5 shows, it is misleading in two ways: a) The use of a pair of crossed lines is incorrect. It must consist of the four <u>independent</u> perpendicular line segments as shown in Figure 2. b) For all but values of s' close to zero, the pair of crossed lines invoked to show irrotational flow, will <u>not</u> necessarily exhibit rates of rotation that will cancel (e.g. the s' = 0.4 case discussed above).

To complete the family of curves in Figure 5, consider the case of s' = 1, when line segment 0i is equal to r_0 and point i coincides with the free vortex singularity at $\theta_i = 180°$. For this limiting case, Equation (14) becomes,

$$\omega_{0i}^*\big|_{s'=1} = \frac{1}{2} - \cos\theta_i , \qquad (16)$$

which is plotted in Figure 5. The area under the s' = 1 curve is nonzero, so this limiting case will yield a nonzero vorticity at point 0.

Equation (14) could also be evaluated for s' > 1, but the results given in Figure 5 for $0 \le s' \le 1$ are sufficient to demonstrate details of vorticity determination by finite line segments about a point in free vortex flow.

Based on the preceding portrayal of a single line segment rotation in free vortex flow, an evaluation of the four element vorticity meter of Figure 2 can now be carried out. Substituting θ_1, $(\theta_1+\pi/2)$, $(\theta_1+\pi)$, and $(\theta_1+3\pi/2)$ into (13) for the four independent line segments in Figure 2, expressions for the velocities at points 1-4 can be put into Equation (7). After some simplification, the nondimensional, spatially-averaged, instantaneous angular velocity, Ω_0^*, for the four line segments in free vortex flow is given by

$$\Omega_0^* = \frac{\Omega_0 r_0^2}{k} = \frac{(s')^2\left[\left((s')^4 - 1\right) + 2\left(\sin 2\phi_0\right)^2\right]}{\left[\left((s')^2 + 1\right)^2\left((s')^2 - 1\right)^2 + 4(s')^4\left(\sin 2\phi_0\right)^2\right]}, \qquad (17)$$

where Ω_0 has been nondimensionalized by k/r_o^2, which can be also interpreted as the average rotation in an area bounded by a circle centered at r = 0 of radius r_0. Equation (17) has been derived for the case of $\theta_1 = 0^o$ (see Figure 2) only, since variation of ϕ_0 between 0^o and 45^o in effect produces a variation of θ_1 at a constant r_0, in the symmetrical free vortex flow field.

The exact value of rotation, ω_0, at point 0 in the free vortex can be obtained by combining (14) with Equation (4) to yield,

$$\omega_0^* = \frac{\omega_0 r_0^2}{k} = \frac{1}{2\pi}\int_0^{2\pi}\left[\frac{1 - \cos\theta\left(s' + 2\cos\theta\right)}{1 + 2s'\cos\theta + \left(s'\right)^2}\right]d\theta, \qquad (18)$$

where ω_0 has been nondimensionalized by k/r_o^2. The integral in (18) was evaluated numerically. However, for the limiting case of s' = 0, the integrand in (18) reduces to (15) directly which yields $\omega_0^* = 0$ (the area under the curve for s' = 0 in Figure 5). Likewise, for the limiting case, of s' = 1, the integrand in (18) becomes (16) which integrates to yields $\omega_0^* = 1/2$ (the area under the curve for s' = 0 in Figure 5).

Figure 6 is a plot of Ω_0^* as a function of s' for various values of ϕ_0, as evaluated from Equation (17), all for $\theta_1 = 0^o$. (The position of the four element vorticity meter or mesh is shown by the insert sketch in the plot.) Also, ω_0^*, the exact value of nondimensional rotation, is shown as a function of s', evaluated by the numerical integration of (18) and the limiting values at s' = 0 and 1. Some important conclusions can be drawn from Figure 6:

i) The nondimensional rotation, ω_0^*, is zero at point 0 for all $0 \le s' < 1$, where the free vortex flow is indeed irrotational. This clearly shows that the calculation or measurement of vorticity by finite line segments (Equation (4)) is independent of s' in this irrotational part of free vortex flow for $0 \le s' < 1$. At s' = 1, the direct effect of the free vortex singularity is made evident by a nonzero rotation, $\omega_0^* = 1/2$.

ii) The angular orientation of the four element vorticity meter (be it a meter (Figure 4) or one element of velocity mesh (Figure 2)) has a strong effect on values of Ω_0^* for s' > 0.2. For instance, at s' = 0.8 for $\phi_0 = 0^o$, $\Omega_0^* = -1.1$ but if at the same point 0, the four element meter or mesh is oriented at $\phi_0 = 45^o$, $\Omega_0^* = 0.4$. The large difference in Ω_0^* between these two angular orientations can be explained by considering the previous detailed discussion of ω_{0i}^* and the plot in Figure 5 for s' = 0.8.

iii) In the irrotational flow, the four element vorticity meter or mesh will essentially indicate zero vorticity (i.e. $\Omega_0^* = 0$) for s' < 0.2 For s' > 0.2 (i.e. for larger finite line elements, s, or smaller distances r_0 from the vortex singularity) the plots in Figure 6 show Ω_0^* values are nonzero (except where a constant ϕ curve crosses the $\Omega_0^* = 0$ axis) in regions of irrotational flow (s'<1.0). In i) above, it was concluded that for $0 \le s' < 1$, the size of the line segment (or the distance of 0 from the singularity) had no effect on the accuracy of the calculated rotation (Equation (4)). Therefore, in Figure 6 it must be concluded that in regions where values of Ω_0^* differ significantly from zero, the inaccuracy is due to n=4, i.e. four line segments (or four points on one opening of a velocity mesh) are not sufficient when s' > 0.2.

This effect of the number of line segments, n, for this free vortex flow can be shown directly by using Equations (6) and (14). Letting $\phi_0 = 0$ and $\theta_1 = 0$, n was varied by evenly distributing line segments about point 0 in multiples of π (e.g. for n=6, $\theta_1 = 0$, $\theta_2 = \pi/3$, $\theta_3 = 2\pi/3$, etc.). Figure 7 shows the results as a plot of Ω_0^* as a function of s' with n as a parameter. For n large ($n=\infty$) a correct value of $\Omega_0^* = 0$ is obtained for all $0 \le s' < 1.0$. The values in Figure 7 show that for n=10, good results ($\Omega_0^* = 0$) are obtained for s' as large as 0.6 , as contrasted with n=4 (Figure 6 and 7) where a vorticity meter or velocity mesh must have s' < 0.2 for accurate estimation of vorticity in this free vortex flow. Very poor accuracy results (as to be expected) occur for n=1, 2, and even n=3.

The reader is cautioned that for n > 4, the point i (Figure 3) does not necessarily coincide with the mesh points in Figure 2. To show the effect this has, consider the mesh points 1–4 and 1' - 4' surrounding point 0 in Figure 2. Involvement of all of these mesh points in a finite difference representation is called a nine-point representation (e.g. see Anderson, Tannehill and Pletcher (1984)), sometimes used to reduce truncation errors in the numerical solution of elliptic partial differential equations. Use of (6), and (17) for points 1-4 (with s') and (17) for points 1' - 4' (with s' replaced by $\sqrt{2}$ s') yields the dashed curve in Figure 7, labeled n' = 8. Comparison of this dashed curve with plot

of n = 8 and n=∞ shows the errors that are introduced by using line segments of different lengths (which is violation of the definition of rotation given earlier for this two-dimensional flow) for a finite difference nine-point representation.

In summary, the steep, concentrated velocity gradients in the free vortex flow have provided the means to draw some conclusions about the effect of vorticity meter (or velocity mesh) size, placement and number of finite line segments on the accurate determination of vorticity.

4) Blasius Boundary Layer Flow

Vorticity determination in a laminar two-dimensional boundary layer formed on a flat plate in an incompressible uniform flow at velocity u_∞ , (see Figure 8) will now be considered. The solution of the boundary layer velocity field, first given by Blasius (e.g., see White (1990)), is not strictly in closed-form, because one must numerically solve the nonlinear ordinary differential equation,

$$f''' + ff'' = 0 \quad , \tag{19}$$

with the boundary conditions, f(0) = 0, f'(0) = 0, and f'(∞) = 1. Tabulated values of f, f' and f'' are given in White (1990) as a function of the similarity parameter, $\eta = y\sqrt{u_\infty / 2\nu x}$ where x and y are shown in Figure 8 and ν is the kinematic viscosity. The streamwise (x) and normal (y) velocities nondimensionalized by u_∞ are,

$$\begin{aligned} \frac{u}{u_\infty} &= f' \\ \frac{v}{u_\infty} &= \sqrt{\frac{\nu}{2u_\infty}}\left(\eta f' - f\right)\frac{1}{\sqrt{x}} \end{aligned} \quad , \tag{20}$$

and the boundary layer thickness (loci of u=0.99 u_∞) is,

$$\delta = 4.925\frac{x}{\sqrt{Re_x}} , \tag{21}$$

where $Re_x = u_\infty x/\nu$ is the boundary layer Reynolds number.

An analytical solution for ζ_0, the transverse or spanwise vorticity in the boundary layer (Figure 8) can be derived from Equation (1), the definition of η, and the velocities in (20) to obtain,

$$\zeta_0 = \frac{u_\infty^{2/3}}{\sqrt{2\nu x}}\left[-f'' + \frac{1}{2\,Re_x}\left\{f - \eta f' - \eta^2 f''\right\}\right], \tag{22}$$

where $\zeta_0 = 2\omega_0$.

If the boundary layer flow considered is restricted to case of $Re_x \geq 10{,}000$, then the Reynolds number coefficient term in (22) is less than 1% of |f''| for values of η in most of the boundary layer, and will be neglected. Equation (22) then becomes,

$$\zeta_0^* = \frac{\zeta_0 \delta}{u_\infty} = -3.483 f'' \ , \tag{23}$$

where ζ_0 has been nondimensionalized by u_∞ and δ (Equation (21)). Equation (19) was solved numerically for f'' and Equation (23) was evaluated to get the plot of ζ_0^* vs. y^* (where $y^* = y / \delta$) shown in Figure 9. The reversed S-shaped curve in Figure 9 shows that the vorticity has a maximum at the wall ($y^* = 0$) and decreases asymptotically to zero just beyond the edge of the boundary layer ($y^* > 1.0$).

The four element vorticity meter or mesh of Figure 2 is shown positioned in the laminar boundary of Figure 8, at point 0 located at (x_0, y_0), and rotated so that $\theta_1 = 0$. Using Equation (7) and defining four-element measured (or calculated) nondimensional vorticity as $Z_o^* = 2\Omega_0\delta/u_\infty$, results in,

$$Z_0^* = \frac{1}{2s^*}\left[\left(\frac{v_1}{u_\infty} - \frac{v_3}{u_\infty}\right) + \left(\frac{u_4}{u_\infty} - \frac{u_2}{u_\infty}\right)\right], \tag{24}$$

where $s^* = s / \delta$. Combining (24) with (20) yields,

$$Z_0^* = \frac{1}{2s^*}\left\{\left(f_4' - f_2'\right) + \left[\frac{1}{\sqrt{2\,Re_{x_1}}}\left(f_1'\eta_1 - f_1\right) - \frac{1}{\sqrt{2\,Re_{x_3}}}\left(f_3'\eta_3 - f_3\right)\right]\right\}. \tag{25}$$

If, as in Equation (23), (25) is limited to $Re_x \geq 10{,}000$ (and $x_0 >> s$), it reduces to,

$$Z_0^* = \frac{1}{2s^*}\left[f'(\eta_4) - f'(\eta_2)\right]. \tag{26}$$

Using a numerical solution of (19), values of f' in (26) were evaluated as a function of $y_0^* = y_0 / \delta$. Figure 9 shows plots of Equation (26) for three values of s^* compared to the exact vorticity distribution in the boundary layer given by Equation (23). Note that none of the s^* curves originate at $y^* = 0$ because of the finite size of the four element configuration. (That is, the nearest position to the wall for $\theta_1 = 0$ is $y_0^* = s^*$).

The agreement with the exact solution (again, for $Re_x \geq 10{,}000$) is excellent for $s^* = 0.1$. The nondimensional vorticity values for a vorticity meter or grid size that is 25% of the boundary thickness ($s^* = 0.25$) are also quite good, with about a maximum of a 3% underprediction of Z_o^* near the wall and a small over prediction of Z_o^* near $y_o^* = 1$. It can be seen from the curve for $s^* = 0.5$ that there are no Z_o^* values obtained near the wall, and in the outer region of the boundary layer, the vorticity meter significantly protrudes into the mainstream flow, causing a serious overprediction of vorticity values.

Thus as in the case of the free vortex flow, Equation (7) provides the means to estimate the maximum size of a four element vorticity meter or velocity grid which should not be exceeded to accurately measure (or calculate) vorticity in a laminar boundary layer.

5) DNS Simulation Analysis

The concept of rotation estimation via multiple line segment tracking was used to analyze the vorticity field created by a flexible thin plate or "flag" (Connell and Yue, 2007). The "true" vorticity field as calculated using a very

fine adaptive mesh is shown in Figure 10 for one time realization. Flow is from left to right and we investigated the field along a line at y = 0 downstream of the foil. The specific flow and structure parameters are, $\mu = 0.3$, $K_b = 0.0001$, Re = 1000, and $K_s = 10$ and represent a plate or flag with high in-plane stiffness and low bending stiffness (refer to Connell and Yue, 2007 for details). First the effect of adding line segments on the estimated vorticity will be assessed as done in Figure 7 for a free vortex and then the effect of increasing the line segment length for an n=4 "meter" will be discussed.

Figure 11 shows the vorticity, ζ, as a function of streamwise distance at y = 0. The "true" vorticity as estimated by a standard 4-point central difference with spacing s of 0.04 is shown for reference and this matched the vorticity as calculated from the adaptive mesh. The vorticity estimated by a "meter" with s = 0.12 and n = 2, 4, and 8, is also shown in Figure 11. Additional line segments clearly improve the vorticity estimate but in regions of steep spatial gradients there is no substitute for small spatial resolution. This is shown by the residual bias error even for larger n and the rms error noted in the figure.

Figure 12 shows the vorticity along the same line as in Figure 11 but for the case of n = 4 line segments and line segment lengths of 3, 5, 7, and 9 times the baseline s = 0.04. Decreasing size clearly improves the estimate of vorticity and decreases rms error. In regions of mild spatial gradients, however, even a "large" meter provides a reasonable estimate of the vorticity. For example for x>2 the estimated vorticity is close to the "true" despite the relatively large "meter" sizes. This is due to the size of the "meter" relative to the vorticity field spatial variations.

CONCLUSIONS

Using a finite line segment approach, expressions have been derived for rotation and vorticity that allow quantitative criteria to be established on how closely a finite-sized device or velocity grid can be expected to yield accurate values of vorticity.

One not surprising conclusion is that the finite size depends on the velocity gradients of the particular flow field under study. Use of the methods presented in this paper should be readily extendible to more complicated, less idealized situations, such as a Rankine vortex, which can approximate such flows as wing-tip vortices (McCormick (1986)) or turbine endwall boundary layer vortices (Langston (1977)).

The introduction of this paper mentioned the general topic of turbulent flow. All of the analytical discussions given here have dealt with laminar flow. However the approach taken should be extendible to turbulent flow. Wyngaard (1969) analyzed the response of a four-wire probe, for varying scales of isotropic turbulence, and recommended probe sizes based on the Kolmogorov length scale. To a first approximation, the probe or element size criteria developed in this paper could also be brought into consideration for a turbulent flow, using the mean flow gradients, in addition to turbulence length scales. An example of the instantaneous turbulent vorticity as estimated by the summation of finite-length line segments was given for different line segment numbers and lengths. The turbulent example was consistent with the analytical laminar examples in that spatial gradients of the velocity field dictate the necessary size of a meter to accurately resolve the vorticity field. Adding line segments or "meter" vanes improves the estimate but only to a point where the finite spatial size of the meter limits the accuracy of the estimated vorticity.

REFERENCES

Anderson, D.A., Tannehill, J.C. and Pletcher, R.H., 1984, Computational Fluid Mechanics and Heat Transfer, Hemisphere, pp. 121-122.

Connell, B. S. H., and Yue, D. K. P., 2007, "The flapping dynamics of a flag in a uniform stream," Journal of Fluid Mechanics, in press.

Kovasznay, L.S.G. 1954, "Section F-Turbulence Measurements", Physical Measurements in Gas Dynamics and Combustion (R.W. Ladenburg, ed), 9, Part 1, pp. 227-228, Princeton Univ. Press.

Lamb, H. 1945, Hydrodynamics, 6th ed., Dover, p 32.

Langston, L.S., Nice, M.L., and Hooper, R.M. 1977, "Three -Dimensional Flow within a Turbine Cascade Passage", J. Engr. Power (Trans. ASME), 99, Jan., pp. 21-28.

McCormick, B.W., Tangler, J.L., and Sherrieb, H .E., 1968, "Structure of Trailing Vortices", J. Aircraft, 5, No. 3, pp. 260-267.

Panton, R.L. 1984, Incompressible Flow, Wiley, pp. 622-627.

Saffman, P.G. 1992, Vortex Dynamics, Cambridge Univ. Press.

Shercliff, J.A. 1977, Vector Fields, , Cambridge Univ. Press. , pp. 204-206.

Truesdell, C. 1954, The Kinematics of Vorticity, pp. 58-61, Indiana Univ. Press.

Wallace, J.M. and Foss, J.F. 1995, "The Measurement of Vorticity in Turbulent Flows", Annu. Rev. Fluid Mech., 27, pp. 469-514.

White, F.M. 1990, Viscous Fluid Flow, 2nd ed., McGraw-Hill, pp. 233-240.

Willey, L.D. 1985, "Aero-Mechanical Measurement of Vorticity in Fluid Flow", SAE Tech. Paper 851894, Aerospace Tech. Conf., Long Beach, CA, pp. 1-12.

Wyngaard, J.C. 1969, "Spatial Resolution of the Vorticity Meter and other Hot-wire Arrays", J. Sci. Instru. (J. Physics E) Series 2, 2, pp. 983-987.

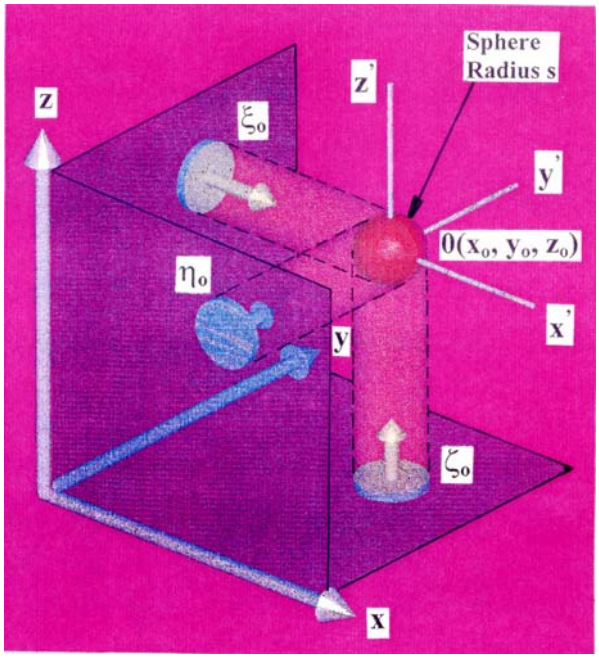

Figure 1. Point (xo, yo, zo) in fluid flow field at instant t. Rotation at 0 is the average relative angular velocity of fluid points on surface of sphere of radius s.

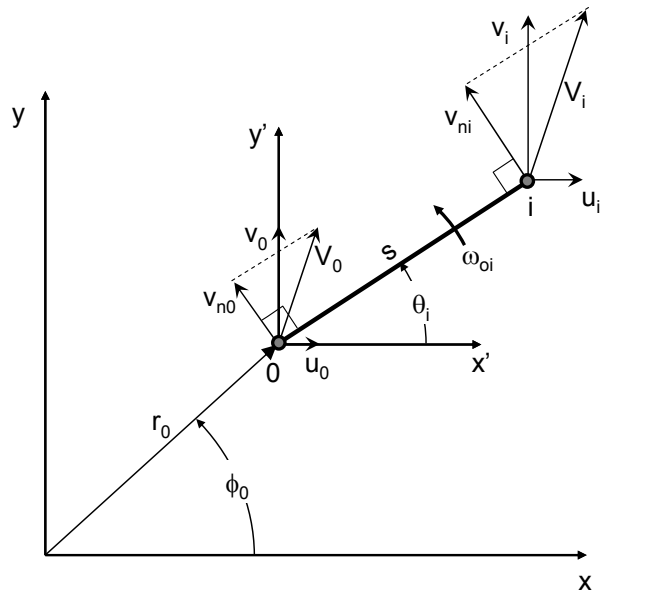

Figure 3. Coordinate system and velocity components used to show rotation of fluid at point i about point 0 as measured by the angular velocity ω_{01} of line segment 0i of length s.

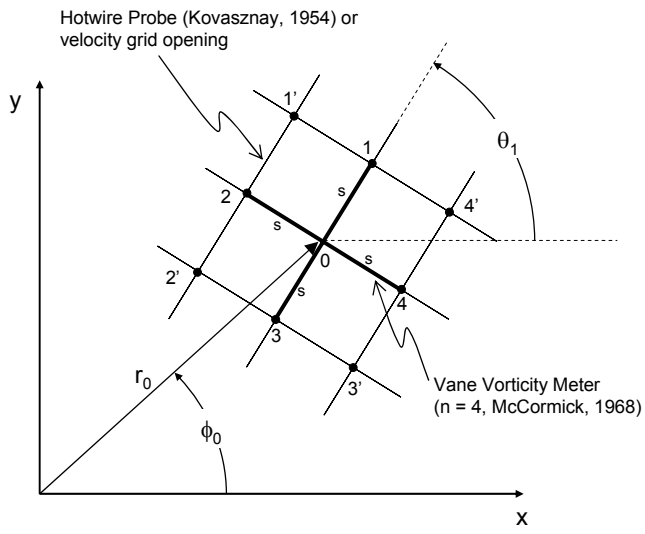

Figure 2. Two-dimensional mesh used for numerical calculations or measurements of velocity. The four independent line segments (01, 02, 03, 04) are used to estimate the rotation at point 0.

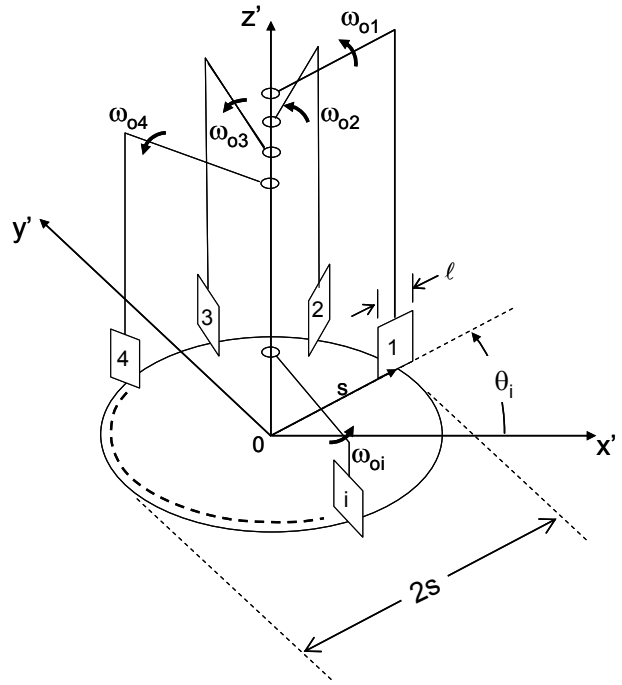

Figure 4. "Ideal" vorticity meter to measure the rotation of fluid at radius s with respect to the z' axis at point 0.

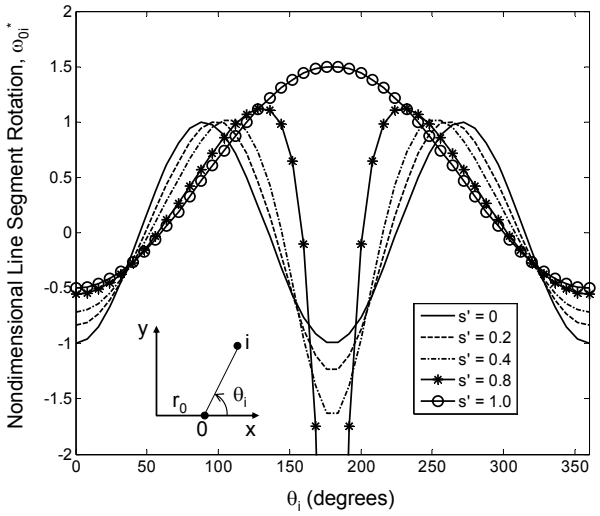

Figure 5. Nondimensional rotation, ω_{0i}^*, of line segment 0i about point 0 in a free vortex as a function of line segment angle θ_i for various values of s' = s / r_0 ($\phi_0 = 0^o$).

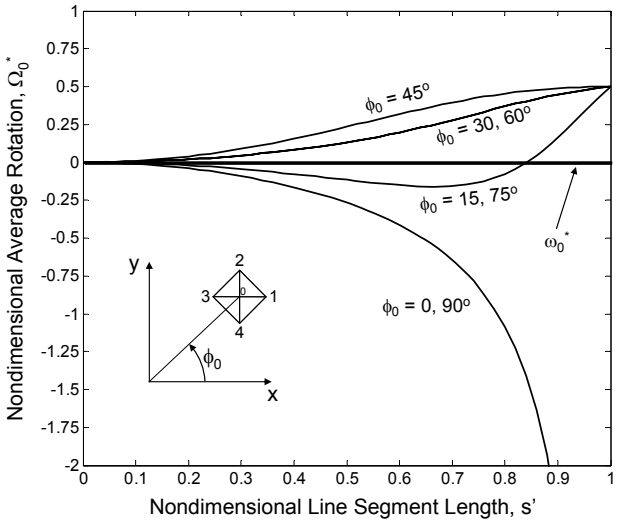

Figure 6. Nondimensional rotation Ω_0^* of fluid about point 0 in a free vortex as a function of s' and ϕ_0, all for $\theta_1 = 0^o$., from Eqn. (17). Bold line is exact solution for rotation, ω_0^*, given by Eqn. (18).

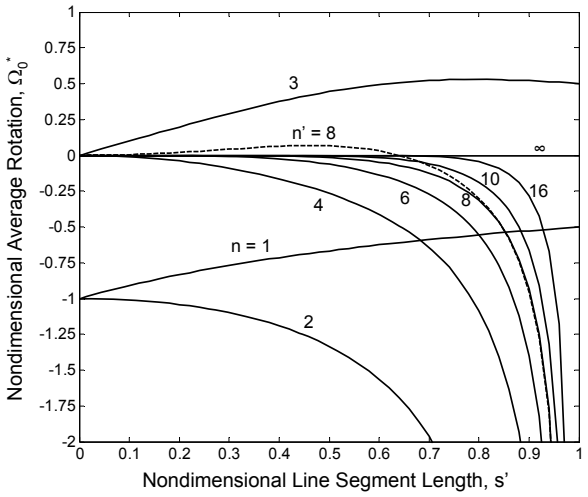

Figure 7. Nondimensional rotation Ω_0^* of fluid about point 0 in a free vortex ($\phi_0 = 0$ and $\theta_1 = 0$) as a function of s'= s/r_0, for values of n, the number of finite line segments. The line segments are evenly distributed about 0 at multiples of $2\pi/n$.

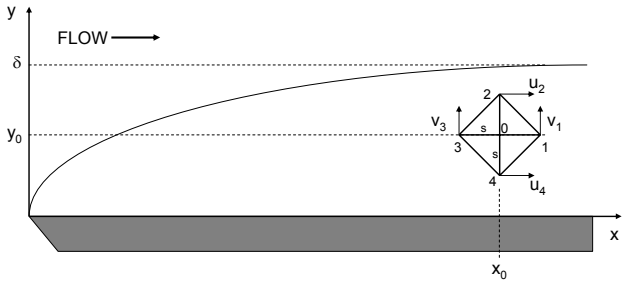

Figure 8. Vorticity determination at a point 0 in a boundary layer with a four-element vorticity meter or velocity grid (for $\theta_1 = 0^o$).

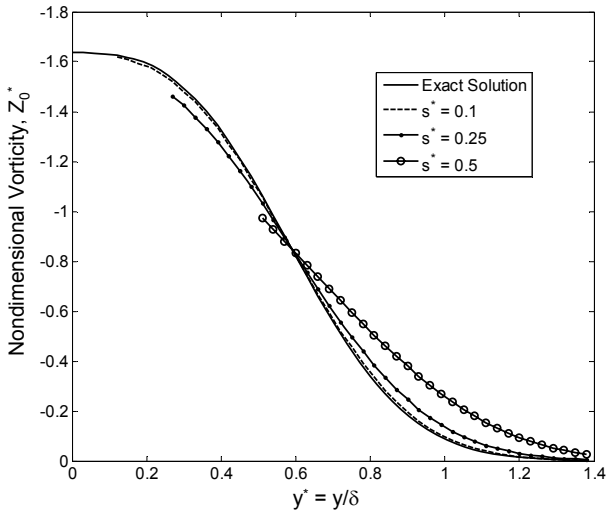

Figure 9. Nondimensional, spanwise vorticity, Z_0^*, in a laminar boundary layer as a function of nondimensional distance from the wall, $y_0^* = y_0/\delta$, and four-element meter size, $s^* = s/\delta$.

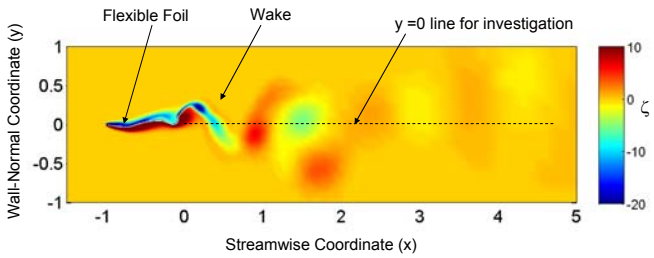

Figure 10. Vorticity Field for Flexible Foil Simulation (Connell and Yue, 2007). Unsteady flow over a 2D flexible thin foil was simulated using DNS.

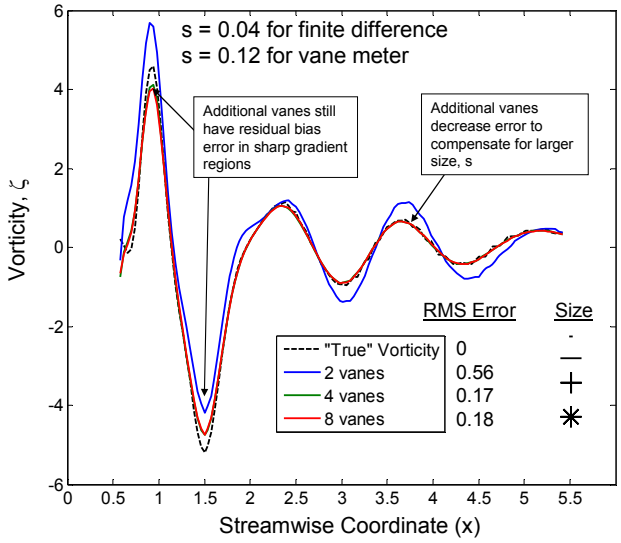

Figure 11. Vorticity along y = 0 line as estimated by conventional 4-point central finite difference and by 2, 4, and 8 line segments with larger vorticity "meter" size

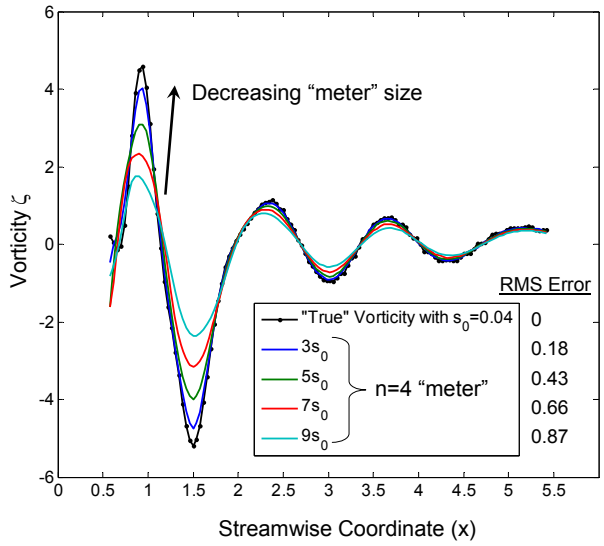

Figure 12. Vorticity along y = 0 line as estimated by conventional 4-point central finite difference and by 4-line segment vorticity "meters" of varying size